PFC/JA-85-20

FINITE TEMPERATURE EFFECTS ON THE SPACE-TIME EVOLUTION OF TWO-STREAM INSTABILITIES*

by

G. Francis, A. K. Ram, and A. Bers

M.I.T. Plasma Fusion Center
Cambridge, MA 02139

July 1985

* This work was supported by the National Science Foundation Grant ECS 82-13430.

Submitted for publication.

FINITE TEMPERATURE EFFECTS ON THE SPACE-TIME EVOLUTION OF TWO-STREAM INSTABILITIES

G. Francis, A. K. Ram, and A. Bers

M.I.T. Plasma Fusion Center

Cambridge, MA 02139

Abstract

Pinch-point instability analysis is used to study the effects of finite temperature on the time-asymptotic pulse shapes of electrostatic and electromagnetic two-stream instabilities. Their absolute or convective instability nature is established over the entire regime from instability threshold at finite temperatures to the cold-plasma hydrodynamic limit. The analysis is based upon Vlasov theory dispersion relations for streams and plasmas with Maxwellian thermal distributions.

PACS numbers: 52.35.Qz, 52.35.Fp, 52.35.Hr

I. Introduction

Linear instability analysis of two-stream interactions is usually carried out by solving the appropriate dispersion relations for complex frequency, ω, as a function of real wavevector, $\overline{k}$. However, this gives very little information about the space-time evolution of such instabilities, e.g. their absolute versus convective nature and their propagation characteristics. These and other such properties must be obtained from a Green's function analysis of the instabilities.[1,2,3] The time-asymptotic Green's function, determined by the pinch-point singularities of the inverse of the dispersion relation, gives the self-similar pulse shapes of the space-time evolution of instabilities. In this paper we present the effects of finite temperature on the space-time evolution of two-stream instabilities based on the kinetic (Vlasov) theory description of the dynamics. This allows us to explore their absolute versus convective nature and propagation characteristics from threshold (Penrose) conditions into the strongly unstable hydrodynamic regime. The cold-plasma, hydrodynamic evolution of electrostatic two-stream instabilities is relatively well-known.[4,5] The evolution of the electromagnetic two-stream instability has not been studied even in the cold-plasma limit. Using the pinch-point analysis we study the time-asymptotic space-time evolution of electrostatic (Pierce-Buneman, beam-plasma) and electromagnetic (Weibel) instabilities generated by two-stream interactions and determine their self-similar pulse shapes as a function of temperature of the plasma and streaming components. The dispersion relations used for the various interactions are based upon the linearized, non-relativistic Vlasov-Maxwell equations for an infinite, homogeneous plasma without any externally applied fields. In the simplest situation, choosing $\overline{k}$ in the direction of maximum growth, the problem can be formulated in one spatial dimension and time; we restrict ourselves to describing such evolutions of two-stream instabilities.

In section II we briefly review the pinch-point analysis used to generate the time-asymptotic pulse shapes of instabilities. In section III we study the evolution of the Pierce-Buneman instability and describe its transition into the ion-acoustic instability. In section IV we determine the propagation velocity of the instability at threshold; as a by-product, we also establish a new method for finding the parameters which give Penrose instability threshold. In section V we study the evolution of the

beam-plasma instability and examine its Penrose instability threshold boundary for different values of the ratio of beam to plasma densities. In section VI we examine the evolution of the electromagnetic, Weibel instability and derive an analytical expression for its pulse-edge velocities. Section VII summarizes the results.

II. Pinch-Point Analysis and Time-Asymptotic Pulse Shapes

To understand the space-time evolution of an instability it is necessary to study the Green's function for the medium. In one dimension, the Green's function is defined as:

$$G(z,t) = \int_L \frac{d\omega}{2\pi} \int_F \frac{dk}{2\pi} \frac{\exp(ikz - i\omega t)}{D(k,\omega)} \tag{1}$$

where $D(k,\omega)$ is the dispersion relation of the system and the Fourier contour (F) and the Laplace contour (L) have been properly chosen to satisfy causality and convergence of the integrals. The time-asymptotic evaluation of (1) is given by the complex pinch points (k_0, ω_0) which are solutions of[6]

$$D(k,\omega) = 0 \quad \text{and} \quad \frac{\partial D}{\partial k} = 0\,. \tag{2}$$

One then finds

$$G(z, t \to \infty) \sim \frac{\exp(ik_0 z - i\omega_0 t)}{t^{1/2}}\,. \tag{3}$$

If the imaginary part of any one pinch point is positive, i.e. $\omega_{0i} > 0$, the instability is absolute, and the time-asymptotic Green's function will be dominated by the pinch point having the largest positive ω_{0i}. On the other hand, if all pinch-point frequencies are in the lower half of the complex ω-plane, i.e. $\omega_{0i} < 0$, the instability is convective.

Of more interest, however, is the space-time shape of the time-asymptotic Green's function – what we shall call the asymptotic pulse shape of the instability. The asymptotic pulse shape is obtained from the Green's function of an observer moving with a velocity V relative to the coordinate system in which $D(k,\omega)$ was derived. An observer moving with a velocity so that he remains inside the unstable pulse response will see an absolute instability. When the observer's velocity is such that he is traveling with the edge of the unstable pulse, the growth rate he sees will be zero. Thus, the

observer's absolute instability growth rate as a function of the observer's velocity gives the time-asymptotic pulse shape of the instability. This can be determined explicitly as follows.

The Green's function in the moving observer's frame is

$$G(z',t) = \int_{L'} \frac{d\omega'}{2\pi} \int_{F'} \frac{dk'}{2\pi} \frac{\exp(ik'z' - i\omega' t)}{D_V(k',\omega')} \tag{4}$$

where for observer velocities much less than the speed of light[7], $D_V(k',\omega',V) = D(k',\omega' + k'V)$ is the dispersion relation in the moving frame. The time-asymptotic evaluation of (4) is given by the pinch-point solution of

$$D_V(k',\omega',V) = 0 \quad \text{and} \quad \frac{\partial D_V}{\partial k'} = 0 \tag{5}$$

which we designate by $[k'_0(V), \omega'_0(V)]$. We then find that relative to the laboratory frame,

$$G(z' = 0, t \to \infty) \sim \frac{\exp[-i\omega'_0(V)t]}{t^{1/2}} \,. \tag{6}$$

Let the unstable pulse shape be given by the logarithmic magnitude of the time-asymptotic Green's function as determined by the pinch-point frequency ω'_0 having the largest positive imaginary part, $\max[\omega'_{oi}(V)]$. Then,

$$\ln|G(t \to \infty)| \sim \max[\omega'_{oi}(V)]t \tag{7}$$

and a plot of $\max[\omega'_{oi}]$ as a function of V determines the (self-similar) unstable pulse shape. If the axes of such a plot are multiplied by t we obtain the time-asymptotic evolution of the unstable pulse, i.e. $\ln|G(t \to \infty)|$ vs. $Vt = z$.

III. Pierce-Buneman Instability

This electrostatic instability of a current carrying plasma is driven by the free energy of electrons streaming through stationary ions.[8,4] We model the unperturbed, neutral plasma in one dimension by a drifting Maxwellian electron distribution and a Maxwellian ion distribution:

$$f_0(v) = n_e \frac{e^{-(v-v_0)^2/v_{the}^2}}{\sqrt{\pi} v_{the}} + n_i \frac{e^{-v^2/v_{thi}^2}}{\sqrt{\pi} v_{thi}} \tag{8}$$

where $v_{the}^2 = 2T_e/m_e$, $v_{thi}^2 = 2T_i/m_i$, $n_e = Z_i n_i$, $T_e(T_i)$, $m_e(m_i)$, and $n_e(n_i)$ are, respectively, the temperature, mass, and particle density of the electrons (ions), and v_0 is the drift velocity of the electrons relative to the ions. The well-known dispersion relation governing the linear dynamics of the system is:

$$D(k,\omega) = 1 - \frac{\omega_{pe}^2}{k^2 v_{the}^2} Z'\left(\frac{\omega - kv_0}{kv_{the}}\right) - \frac{\omega_{pi}^2}{k^2 v_{thi}^2} Z'\left(\frac{\omega}{kv_{thi}}\right) = 0 \tag{9}$$

where $\omega_{pe}^2 = (e^2 n_e/m_e\epsilon_0)$, $\omega_{pi}^2 = (Z_i e^2 n_e/m_i\epsilon_0)$, and $Z'(x)$ is the derivative of the plasma dispersion function with respect to its argument.

In the cold-plasma limit ($v_{the} = v_{thi} = 0$) the space-time evolution is that of an absolute instability; the leading edge of the pulse moving at the electron drift velocity v_0 and the trailing edge fixed at the spatial origin of the initial perturbation[4] (see Fig. 1). This type of space-time evolution can be described as absolute in a half-space, since it expands to fill only the half space, to one side of the origin, in the direction of the drifting species. The Pierce-Buneman instability changes to a convective one and actually moves away from the origin as soon as a thermal spread is added to the ions (see Fig. 1). To understand this behavior it is useful to visualize the pulse as a superposition of wavepackets having group velocities, v_g, ranging continuously from $v_g = 0$ to $v_g = v_0$. For ions having a finite thermal spread, the wavepackets with low group velocities are Landau damped on the ion distribution. The maximum spatial growth rate of the convective instability is given by the slope of the line that is tangent to the pulse and passes through the origin[1-3] (see Fig. 1). Keeping $v_{the} = 0$, as v_{thi} is increased, increasingly faster wavepackets are damped away and the growth rate for the instability decreases until it becomes negligible (reduced in amplitude by several orders of magnitude) for $v_{thi} \approx 0.3v_0$. As predicted by Penrose,[9] the system will never become entirely stabilized as long as we assume that the electrons have a delta function distribution at v_0.

If the ions are kept cold and the electron temperature is increased, the instability remains absolute and its growth is reduced in a completely different manner. The

wavepackets in the pulse that have group velocities near v_0, being made up of negative energy waves (in a frame moving with the electron drift), are Landau damped on the broadening electron distribution, thereby slowing down the leading edge of the pulse (see Fig. 2). This slowing down of the pulse continues with increasing v_{the} until the leading edge velocity of the pulse meets the increasing ion-sound velocity $c_s = (Z_i T_e/m_i)^{1/2}$ at $v_{the} \approx 1.5 v_0$. A further increase in v_{the} changes the instability into a new mode – the ion-acoustic instability – where the growing wavepackets are positive energy waves (of the electron-ion system) near c_s driven unstable by anti-Landau damping on the electron distribution function below v_0. The leading edge of the pulse then begins to speed up and remains slightly faster than the ion-sound velocity (see Fig. 3). Note that the ion-acoustic mode is a much weaker instability; the amplitude of its pulse (which is the logarithm of its response function) being more than an order of magnitude smaller than that of the cold Pierce-Buneman instability. In this ion-acoustic regime ($v_{the} > 1.5 v_0$), an increase in the ion temperature not only changes the instability into a convective one, by ion-Landau-damping the low velocity portion of the pulse, but it also speeds up the leading edge slightly due to the ion thermal corrections to the ion-sound velocity ($c_s = [(Z_i T_e + 3T_i)/m_i]^{1/2}$, see Fig. 4). For the particular case depicted in Fig. 4 where $v_{the} = 5.0 v_0$, the system becomes (Penrose) stable at $v_{thi} = 0.055\, v_0$. Thus, for finite v_{the} and v_{thi} the ion-acoustic instability is convective at threshold.

IV. Propagation Velocity at Instability Threshold

The Penrose criteria for instability[9], which are normally used to determine the instability threshold boundary, are: that the weighted velocity distribution function

$$\varphi_{ei}(v) = e^{-(v-v_0)^2/v_{the}^2} + N_{ie} T_{ei}^{1/2} e^{-v^2/v_{thi}^2} \tag{10}$$

have a relative minimum at $v = v_{\min}$; and that the Penrose function

$$I_{ei}(v) \equiv Z'\left(\frac{v - v_0}{v_{the}}\right) + N_{ie} T_{ei} Z'\left(\frac{v}{v_{thi}}\right) \tag{11}$$

be positive for $v = v_{\min}$, where $N_{ie} \equiv \omega_{pi}^2/\omega_{pe}^2$ and $T_{ei} \equiv v_{the}^2/v_{thi}^2$. The two conditions are the necessary and sufficient conditions, respectively, for the existence of an instability. Although $I_{ei}(v)$ is in general a complex quantity, $I_{ei}(v_{\min})$ is real since the

imaginary part of $I_{ei}(v)$ is just the derivative of the weighted distribution function with respect to velocity.

The Penrose instability threshold boundary for the Pierce-Buneman instability is plotted in Figures 5a and 5b. Because of the temperature dependence of the vertical and horizontal axes, both plots are necessary to effectively visualize the instability threshold. Figure 5a is useful when the electron temperature is kept constant and the ion temperature is varied. Figure 5b is useful when the ion temperature is kept constant. Note that each of the curves in Figure 5 is divided into three regions by two dots. In the region between the two dots the appearance of a relative minimum in $\varphi_{ei}(v)$ is not enough to cause instability - the minimum must be deep enough to cause $I_{ei}(v_{\min}) > 0$ before the onset of instability. In the regions exterior to the two dots $I_{ei}(v_{\min})$ is already positive when the relative minimum first appears. Therefore, the criterion for the onset of instability in these regions is just the appearance of a saddle point, i.e. $\varphi'_{ei}(v_{\min}) = \varphi''_{ei}(v_{\min}) = 0$.

We now use the pinch-point analysis to determine the propagation velocity of the Pierce-Buneman instability at threshold. This method also provides an alternative means of generating the Penrose instability threshold boundary. The pinch-point solutions of Eqs. (5) satisfy the relation[1]

$$\frac{d\omega'_0(V)}{dV} = -k'_0(V)\,. \tag{12}$$

The maximum temporal growth rate of the time-asymptotic pulse shape therefore occurs at an observer velocity $V = V_0$ such that $k'_0(V_0)$ is a real quantity, since

$$-k'_{0i}(V_0) = \frac{d\omega'_{0i}(V_0)}{dV} = 0\,. \tag{13}$$

The maximum temporal growth rate of the instability may be found for given values of the parameters v_0, T_{ei}, and N_{ie}, by solving Eqs. (5) for the four unknowns $\omega'_0(V_0) = \omega'_{0r}(V_0) + i\omega'_{0i}(V_0)$, $k'_{0r}(V_0)$, and V_0. Instead of solving for this maximum temporal growth rate, $\omega'_{0i}(V_0)$, we choose to specify it as a positive-valued parameter and then solve Eqs. (5) for the real parts of the pinch point $[k'_{0r}(V_0), \omega'_{0r}(V_0)]$, V_0, and v_0; all as functions of the parameters $\omega'_{0i}(V_0)$, T_{ei}, and N_{ie}. If we then take the limit $\omega'_{0i}(V_0) \to 0$ (instability threshold), the solution of Eqs. (5) for V_0 is the propagation

velocity of the instability at threshold – what we shall call the threshold convection velocity, V_c. As shown by a detailed derivation given in the appendix, this threshold convection velocity is given by

$$V_c = v_{\min} + 2\left[\frac{I_{ei}(v_{\min})}{dI_{ei}(v_{\min})/dv}\right]. \tag{14}$$

In the regions outside of the two dots on the Penrose boundary, $I_{ei}(v_{\min})$ and $dI_{ei}(v_{\min})/dv$ are real and nonzero. In the region between the dots $I_{ei}(v_{\min}) = 0$ at threshold and $V_c = v_{\min}$, i.e. the threshold convection velocity is just the velocity of the relative minimum in the weighted distribution function. It should be noted that for a large range of usual parameters ($2.5 < T_e/T_i < 20$) in the ion-acoustic regime, V_c as given by Eq. (14) is within 5% of c_s. This is exactly as expected.

The solution of Eqs. (5) for v_0 as a function of $\omega'_{0i}(V_0)$, T_{ei}, and N_{ie} allows us to map out contours of constant maximum temporal growth rate in the space spanned by the relevant parameters. Stringer[10] first produced such a contour plot for the Pierce-Buneman instability using a rather tedious method. He repeatedly plotted the dispersion relation as a function of real wavenumbers for different values of T_{ei} and v_0. For each of the curves he located the maximum temporal growth rate and then interpolated to produce his contour plot. The pinch-point method described here makes such a tedious calculation unnecessary. Further, if we take the limit $\omega'_{0i}(V_0) \to 0$, we get the Penrose instability threshold boundary.

V. Electron Beam-Plasma Instability

This electrostatic instability occurs when a (low-density) electron beam is made to drift through a (high-density) quasi-neutral plasma. In describing this two-stream interaction the ion dynamics are ignored (the characteristic frequencies being sufficiently high to justify this) and the relevant distribution function for the system of electron beam and plasma electrons is taken as:

$$f_0(v) = n_b \frac{e^{-(v-v_0)^2/v_{thb}^2}}{\sqrt{\pi} v_{thb}} + n_p \frac{e^{-v^2/v_{thp}^2}}{\sqrt{\pi} v_{thp}}. \tag{15}$$

Here $v_{thb}^2 = 2T_b/m_e$, $v_{thp}^2 = 2T_p/m_e$, $T_b(T_p)$ and $n_b(n_p)$ are, respectively, the temperature and particle density of the beam (plasma) electrons, and v_0 is the drift

velocity of the beam. The ions are assumed to form an infinitely massive, neutralizing background. The resulting dispersion relation is:

$$D(k,\omega) = 1 - \frac{\omega_b^2}{k^2 v_{thb}^2} Z'\left(\frac{\omega - kv_0}{kv_{thb}}\right) - \frac{\omega_p^2}{k^2 v_{thp}^2} Z'\left(\frac{\omega}{kv_{thp}}\right) = 0 \qquad (16)$$

where $\omega_b^2 = (n_b e^2/m_e\epsilon_0)$ and $\omega_p^2 = (n_p e^2/m_e\epsilon_0)$.

The beam-plasma instability is similar to the Pierce-Buneman instability in many mathematical respects, but physically the two are very different. Like the Pierce-Buneman instability, its asymptotic space-time evolution, or pulse shape, is half-absolute in the cold-plasma limit; the leading edge moving at the drift velocity of the beam.[5] When the temperature of the drifting species (the beam) is increased while keeping the stationary species (the plasma electrons) cold, the pulse remains absolute while it slows down (see Fig. 6), just as the Pierce-Buneman pulse shape did when the temperature of the drifting electrons was increased. (This effect has also been shown analytically using a Lorentzian distribution to model the beam electrons.[11]) However, here the wavepackets in the pulse that have group velocities near v_0 are negative energy waves (in the plasma frame) associated with the electron beam; they become Landau damped as the beam temperature becomes nonzero. Increasing the temperature of the plasma electrons causes the low velocity portion of the pulse to be Landau-damped, and the instability becomes convective (see Fig. 7). For sufficient temperatures in both the beam and the plasma electrons the instability is in the so-called "bump-on-tail" kinetic regime; here, the convectively unstable wavepackets are positive energy plasma waves driven unstable by anti-Landau damping on the beam distribution below v_0.

The Penrose instability threshold boundary is plotted for several values of the ratio of the plasma density to the beam density ($N \equiv n_p/n_b$) in Figures 8a and 8b. Figure 8a is to be used when the beam temperature is kept constant and the plasma temperature is varied. Figure 8b is useful when the plasma temperature is kept constant. The Penrose conditions for instability in this case are: that the weighted velocity distribution function

$$\varphi_{bp}(v) = e^{-v^2/v_{thp}^2} + N_{bp} T_{pb}^{1/2} e^{-(v-v_0)^2/v_{thb}^2} \qquad (17)$$

have a relative minimum at $v = v_{\min}$; and that the Penrose function

$$I_{bp}(v) \equiv Z'\left(\frac{v}{v_{thp}}\right) + N_{bp}T_{pb}Z'\left(\frac{v - v_0}{v_{thb}}\right) \tag{18}$$

be positive for $v = v_{\min}$, where $N_{bp} = \omega_b^2/\omega_p^2$ and $T_{pb} = v_{thp}^2/v_{thb}^2$.

It is interesting to note the symmetry between $\varphi_{bp}(v + v_0)$ and $\varphi_{ei}(v)$. Indeed, it can be shown that the beam-plasma instability threshold boundary in the space spanned by v_0/v_{thp} and T_{pb} is identical to that of the Pierce-Buneman in the space spanned by v_0/v_{the} and T_{ei}, provided that $N_{ie} = N_{bp}$. (This symmetry breaks down when the ion dynamics can no longer be ignored in the beam-plasma interaction.)

As before, each of the curves in Figures 8a and 8b is divided into three regions by two dots. The region between the dots again requires a deep enough minimum in the weighted distribution function to cause an instability. The external regions require only the presence of a minimum.

Using the method presented in section IV and in the appendix, we find the threshold convection velocity for the beam-plasma instability to be

$$V_c = v_{\min} + 2\left[\frac{I_{bp}(v_{\min})}{dI_{bp}(v_{\min})/dv}\right]. \tag{19}$$

In the regions outside of the two dots on the Penrose boundary both $I_{bp}(v_{\min})$ and $dI_{bp}(v_{\min})/dv$ are real and nonzero. In the region between the dots $I_{bp}(v_{\min}) = 0$ at threshold and $V_c = v_{\min}$, just as in the case of the Pierce-Buneman instability.

VI. Electron-Weibel Instability

This electromagnetic instability may be driven by either counter-streaming beams of electrons or by a temperature anisotropy,[12] or both. We allow for either of these mechanisms by defining the three-dimensional velocity space distribution function to be:

$$f_0(v_E, v_B, v_k) = \frac{e^{-v_B^2/v_{tB}^2}e^{-v_k^2/v_{tk}^2}}{\pi^{3/2}v_{tE}v_{tB}v_{tk}}\left\{\frac{e^{-(v_E - v_0)^2/v_{tE}^2} + e^{-(v_E - v_0)^2/v_{tE}^2}}{2}\right\} \tag{20}$$

where v_{tE}, v_{tB}, and v_{tk} are the thermal velocities in the direction of the perturbed electromagnetic wave electric field ($\overline{E}_1$), magnetic field ($\overline{B}_1$), and propagation vector ($\overline{k}$), respectively. If we ignore the ion dynamics, the resulting dispersion relation is:

$$D(k,\omega) = 1 - \frac{k^2c^2}{\omega^2} - \frac{\omega_{pe}^2}{\omega^2} - \frac{\omega_{pe}^2}{\omega^2}\frac{(v_{tE}^2 + 2v_0^2)}{2v_{tk}^2} Z'\left(\frac{\omega}{kv_{tk}}\right) = 0 \qquad (21)$$

where ω_{pe} is the electron plasma frequency, c is the speed of light.

The $\overline{v} \times \overline{B}_1$ force serves as the feedback mechanism through which any anistropic thermal spread (v_{tE}) or any streaming (v_0) along the $\overline{E}_1$ direction drives the system unstable.[13] Likewise, the $\overline{v} \times \overline{B}_1$ force causes the wave to be damped by any thermal spread (or counter-streaming) in the direction of $\overline{k}$. Thermal spread and counter-streaming in the direction of $\overline{B}_1$ have no effect on this instability.

In the cold-plasma limit ($v_{tE} = v_{tB} = v_{tk} = 0$) where the Weibel instability is driven by streaming alone ($v_0 \neq 0$), its space-time evolution is that of an absolute instability (see Fig. 9) which is symmetric about the spatial origin of the initial perturbation, which is to be expected. The leading edges of the pulse move out at velocities $\pm v_0$, which we would not expect as the unstable pulse propagates in the $\overline{k}$-direction which is perpendicular to the counter-streaming beams. The cold-plasma pulse has infinite slope for zero observer velocity, indicating that the pinch point occurs for $|k_0| \to \infty$. For non-zero v_{tk} the pinch point for zero observer velocity moves into the finite complex k-plane and the slope of the pulse at the origin becomes finite. Further increase in the temperature along the direction of propagation drives the system towards stability, and the unstable pulse disappears when $v_{tk}^2 > 2v_0^2 + v_{tE}^2$.

If the electrons are cold along the direction of propagation of the wave ($v_{tk} = 0$), then it is possible to derive an analytical expression for the pulse-edge velocities, V_{pe}. In the laboratory frame we solve the following system of equations:

$$\begin{aligned} &D(k_0,\omega_0) = 0 \\ &\frac{\partial D}{\partial k} + V_{pe}\frac{dD}{d\omega} = 0 \\ &\omega_{0i} - V_{pe}k_{0i} = 0 \end{aligned} \qquad (22)$$

for the three unknowns: k_0, ω_0, and V_{pe}. The resulting pulse-edge velocities are:

$$V_{pc}^2 = v_0^2 + v_{tE}^2/2 \tag{23}$$

where terms of order $(v_0^2 + v_{tE}^2/2)/c^2$ have been neglected, consistent with our nonrelativistic analysis and dispersion relation (21).

VII. Summary and Discussion of Results

We have used pinch-point instability analysis to investigate the effects of finite temperature on the space-time evolution of three different two-stream instabilities: the Pierce-Buneman, the electron beam-plasma, and the electron Weibel instabilities. While all three are shown to be absolute instabilities in the cold-plasma, hydrodynamic limit, the two electrostatic instabilities become convective when the stationary particle species acquires a finite temperature. The transition of the Pierce-Buneman instability into the ion-acoustic regime of parameter space was shown to be associated with a change in behavior of the time-asymptotic pulse shape with increasing electron temperature. At the transition, $v_{the} \approx 1.5 v_0$, the leading edge of the unstable pulse stopped its slowing down (behavior characteristic of the Pierce-Buneman instability with increasing electron temperature), and began instead to speed up with increasing electron temperature, remaining slightly faster than the increasing ion-sound velocity.

At instability threshold the pinch-point analysis was used to determine the convection velocity of the instability. This also gave new means for finding the Penrose instability threshold boundary in the relevant parameter space. Analytical expressions for the threshold convection velocities were found for the electrostatic Pierce-Buneman (Eq. 14) and electron beam-plasma (Eq. 19) instabilities. Both of these instabilities are convective at their instability threshold with finite temperature in the stationary and streaming particle species. Since all experiments take place within a finite volume, this threshold convection velocity allows one to estimate whether the instability near threshold will have had enough time to grow to significant amplitudes before reaching the boundaries.

The electromagnetic, counter-streaming electron Weibel instability was found to be absolute at threshold and above. Its maximum pulse-edge velocities correspond to energies characteristic of the total (drift plus thermal) free energy which drives the instability.

VIII. Acknowledgments

The authors are pleased to acknowledge several very helpful discussions with Dr. Gary R. Smith of Lawrence Livermore National Laboratories regarding the use of his plasma dispersion function code.

This work was supported by the National Science Foundation Grant ECS 82-13430.

Appendix: Derivation of V_c

We solve equations (5):

$$\begin{aligned} D_{V_0}(k'_{0r}, \omega'_{0r}, V_0, v_0; \omega'_{0i}, T_{ci}, N_{ie}) &= 0 \\ \frac{\partial D_{V_0}}{\partial k'}(k'_{0r}, \omega'_{0r}, V_0, v_0; \omega'_{0i}, T_{ei}, N_{ie}) &= 0 \end{aligned} \tag{A1}$$

for the real parts of the pinch point $[k'_{0r}(V_0), \omega'_{0r}(V_0)]$, observer velocity of maximum temporal growth V_0, and drift velocity v_0 as functions of the parameters $\omega'_{0i}(V_0)$, T_{ei}, and N_{ie}. Equations (A1) can be written in terms of the Penrose function $I_{ei}(v)$, Eq. (11), as:

$$I_{ei}(v'_{ph} + V_0) = \kappa^2 \tag{A2}$$

$$v'_{ph} \frac{dI_{ei}(v'_{ph} + V_0)}{dv} = -2\kappa^2 \tag{A3}$$

where $v'_{ph} \equiv [\omega'_{0r}(V_0) + i\omega'_{0i}(V_0)]/k'_{0r}(V_0)$ and $\kappa \equiv k'_{0r}(V_0)v_{the}/\omega_{pe}$. These equations are most easily solved for V_0 by transforming them into the laboratory frame of reference, where they become:

$$I_{ei}(v_{ph}) = \kappa^2 \tag{A4}$$

$$(v_{ph} - V_0) \frac{dI_{ei}(v_{ph})}{dv} = -2\kappa^2 \tag{A5}$$

where $v_{ph} \equiv [\omega_{0r}(V_0) + i\omega'_{0i}(V_0)]/k'_{0r}(V_0) = v'_{ph} + V_0$. Solving for V_0, we get

$$V_0 = v_{ph} + 2\left[\frac{I_{ei}(v_{ph})}{dI_{ei}(v_{ph})/dv}\right]. \tag{A6}$$

In the limit $\omega'_{0i}(V_0) \to 0$, the imaginary portions of equations (A4) and (A5) can be written in terms of the weighted distribution function $\varphi_{ei}(v)$, Eq. (10), as:

$$\varphi'_{ei}(v_{ph}) = 0 \quad , \quad \varphi''_{ei}(v_{ph}) = 0\,. \tag{A7}$$

Hence, in the regions outside of the two dots on the Penrose boundary (Figure 5), equations (A7) yield $v_{ph} = v_{\min}$, and in these regions Eq. (A6) becomes Eq. (14):

$$V_c = v_{\min} + 2\left[\frac{I_{ei}(v_{\min})}{dI_{ei}(v_{\min})/dv}\right]. \qquad (A8)$$

In the region between the two dots on the Penrose boundary it can be shown that the pinch point $[k'_{0r}(V_0), \omega'_0(V_0)]$ giving maximum temporal growth rate goes to zero as threshold is approached in such a way that v'_{ph} also goes to zero. In this central region, taking the limit $\omega'_{0i}(V_0) \to 0$ in Eq. (A4) yields

$$I_{ei}(V_c) = 0\,. \qquad (A9)$$

Comparing this to the second Penrose condition for instability threshold, we find that $V_c = v_{\min}$ in the region between the two dots. Equation (14) for the threshold convection velocity is, therefore, valid for all values of the parameters T_{ei} and N_{ie}.

References

1. R. J. Briggs, *Electron Stream Interaction with Plasmas*, (MIT Press, Cambridge, Mass., 1964).

2. L. S. Hall and W. Heckrotte, Phys. Rev. 166, 120 (1968).

3. A. Bers, "Space-Time Evolution of Plasma Instabilities – Absolute and Convective" in *Handbook of Plasma Physics* (gen. eds. M. W. Rosenbluth and R. Z. Sagdeev), *Vol. 1, Basic Plasma Physics* (vol. eds. A. A. Galeev and R. N. Sudan), Chapter 3.2, (North Holland Publ. Co., Amsterdam, Holland, 1983).

4. O. Buneman, Phys. Rev. 115, 503 (1960).

5. R. J. Briggs, in *Advances in Plasma Physics, Vol. 4*, Edited by A. Simon and W. B. Thompson, (John Wiley & Sons, Inc., New York, 1971), p. 43.

6. Note that not all solutions of (2) are pinch points; also, pinch points occurring for $k \to \infty$ must be dealt with seperately. For further details see Ref. 3.

7. For a relativistically correct treatment of pinch-point analysis in three dimensions, see A. Bers, A. K. Ram, and G. Francis, Phys. Rev. Lett. 53, 1457 (1984).

8. J. R. Pierce, Jour. Appl. Phys. 19, 231 (1948).

9. O. Penrose, Phys. Fluids 3, 258 (1960).

10. T. E. Stringer, Plasma Physics (Jour. Nuclear Energy Part C) 6, 267 (1964).

11. Michael E. Jones and Don S. Lemons, Bull. Am. Phys. Soc. 28, 1258 (1983).

12. E. S. Weibel, Phys. Rev. Lett. 2, 83 (1959).

13. F. F. Chen, *Introduction to Plasma Physics and Controlled Fusion*, 2nd ed., (Plenum Press, New York, 1984).

Figure Captions

Figure 1 – Effect of increasing $v_i \equiv v_{thi}/v_0$ on the Pierce-Buneman time-asymptotic pulse shape. The electrons are kept cold ($v_e \equiv v_{the}/v_0 = 0$). Hydrogen plasma is assumed.

Figure 2 – Effect of increasing $v_e \equiv v_{the}/v_0$ on the Pierce-Buneman pulse shape. The ions are kept cold.

Figure 3 – Effect of increasing $v_e \equiv v_{the}/v_0$ on the ion-acoustic pulse shape. The ions are kept cold. The leading edge of the pulse travels slightly faster than the ion-sound speed, $c_s = (T_e/m_i)^{1/2}$.

Figure 4 – Evolution of ion-acoustic pulse shape with increasing $v_i \equiv v_{thi}/v_0$ for a fixed value of v_{the} ($v_{the} = 5.0v_0$). The ion-sound speed is: $c_s = [(T_e + 3T_i)/m_i]^{1/2}$.

Figure 5 – Penrose instability threshold boundary of the Pierce-Buneman instability: a) as a function of ion temperature for fixed electron temperature, and b) as a function of electron temperature for fixed ion temperature. Hydrogen plasma is assumed. Our results agree with the curve given by Penrose.[9]

Figure 6 – Effect of increasing $v_b \equiv v_{thb}/v_0$ on the beam-plasma pulse shape. The plasma is kept cold ($v_p \equiv v_{thp}/v_0 = 0$). A weak beam is assumed ($n_p/n_b = 1836$). Ion dynamics have been ignored.

Figure 7 – Effect of increasing $v_p \equiv v_{thp}/v_0$ on the beam-plasma pulse shape. The beam is kept cold. $n_p/n_b = 1836$.

Figure 8 – Penrose instability threshold boundary of the electron beam-plasma instability for different values of the relative beam density ($N \equiv n_p/n_b$): a) as a function of plasma temperature for fixed beam temperature, and b) as a function of beam temperature for fixed plasma temperature.

Figure 9 – Evolution of the electron Weibel instability pulse shape with increasing temperature (v_{tk}) along the direction of wave propagation $\overline{k}$. The counter-streaming electron beams are taken to have drift velocities $v_0 = \pm 0.1c$, respectively, perpendicular to $\overline{k}$. Temperature perpendicular to $\overline{k}$ is assumed zero.

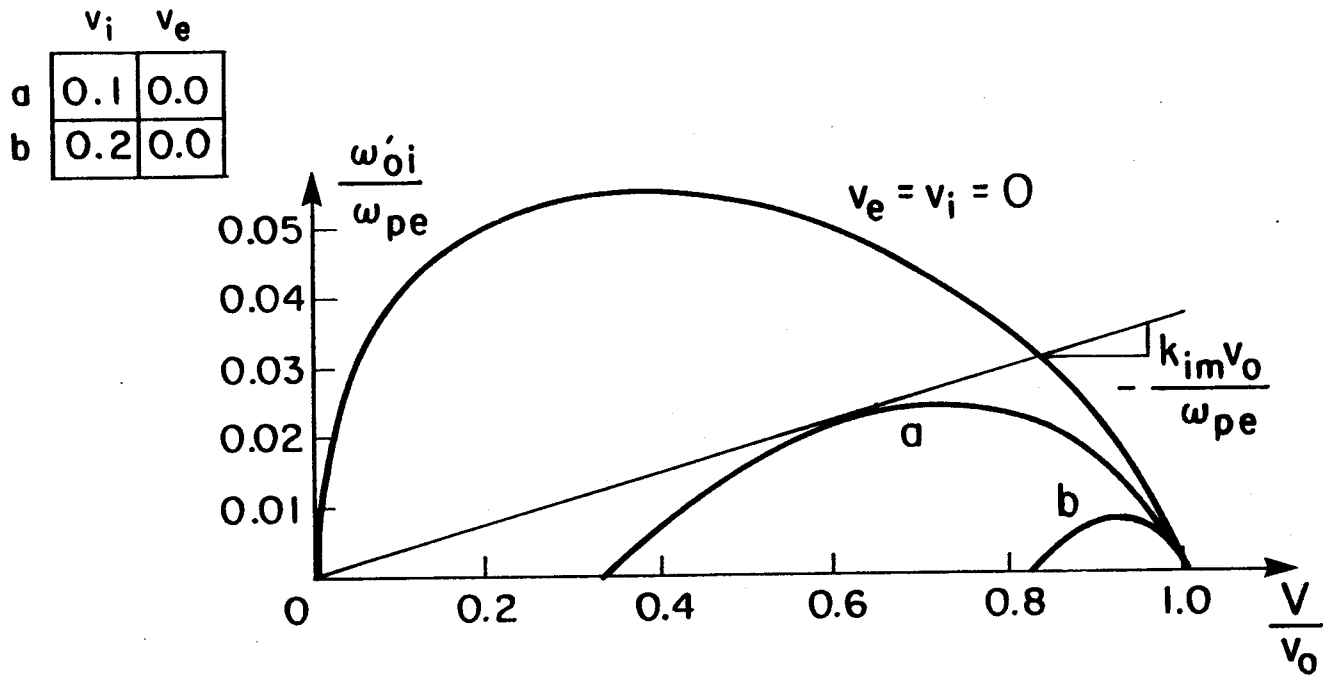
v_i v_e
a 0.1 0.0
b 0.2 0.0
$\frac{\omega'_{oi}}{\omega_{pe}}$
0.05
0.04
0.03
0.02
0.01
0
0.2
0.4
0.6
0.8
1.0
$\frac{V}{V_o}$
$v_e = v_i = 0$
$-\frac{k_{im}v_o}{\omega_{pe}}$
a
b

FIGURE 1

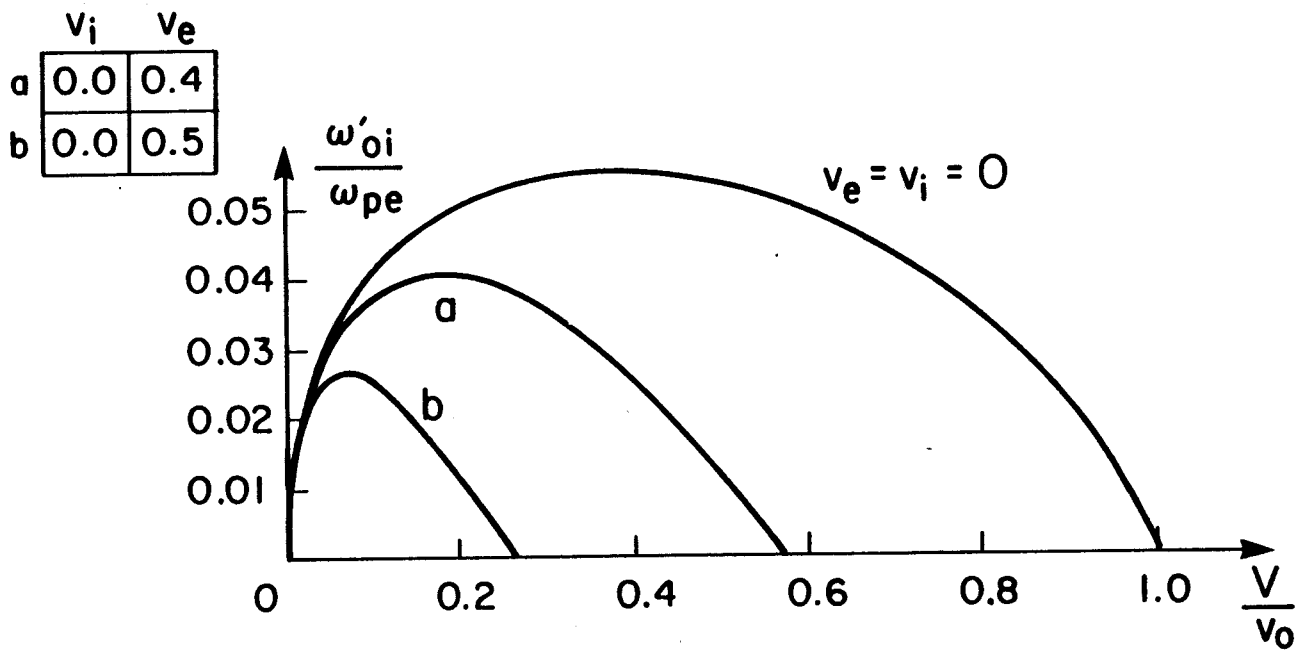
v_i v_e
a 0.0 0.4
b 0.0 0.5
$\frac{\omega'_{oi}}{\omega_{pe}}$
0.05
0.04
0.03
0.02
0.01
0
0.2
0.4
0.6
0.8
1.0
$\frac{V}{v_o}$
$v_e = v_i = 0$
a
b

FIGURE 2

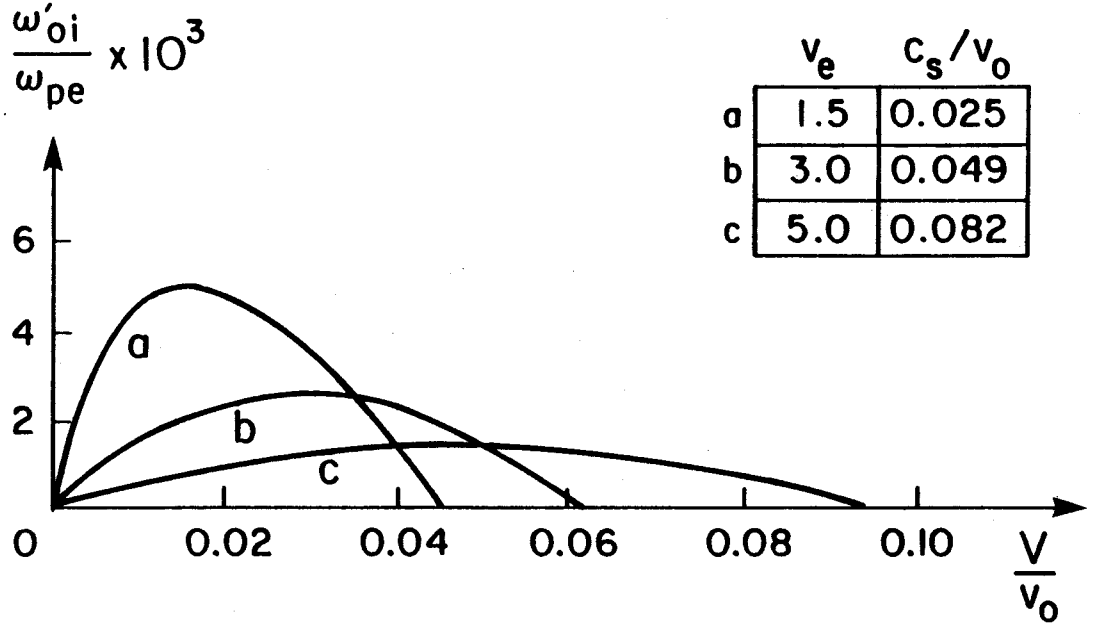
$\frac{\omega'_{oi}}{\omega_{pe}} \times 10^3$
v_e c_s/v_o
a 1.5 0.025
b 3.0 0.049
c 5.0 0.082
6
4
2
0
a
b
c
0.02
0.04
0.06
0.08
0.10
$\frac{V}{v_o}$

FIGURE 3

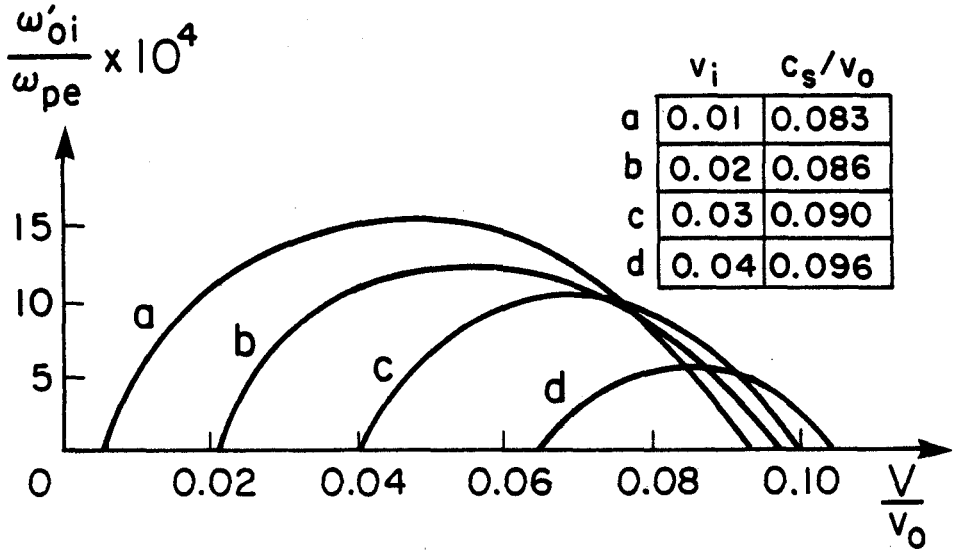
$\frac{\omega'_{oi}}{\omega_{pe}} \times 10^4$
15
10
5
0
0.02
0.04
0.06
0.08
0.10
$\frac{V}{V_o}$
a
b
c
d
v_i c_s/v_o
a 0.01 0.083
b 0.02 0.086
c 0.03 0.090
d 0.04 0.096

FIGURE 4

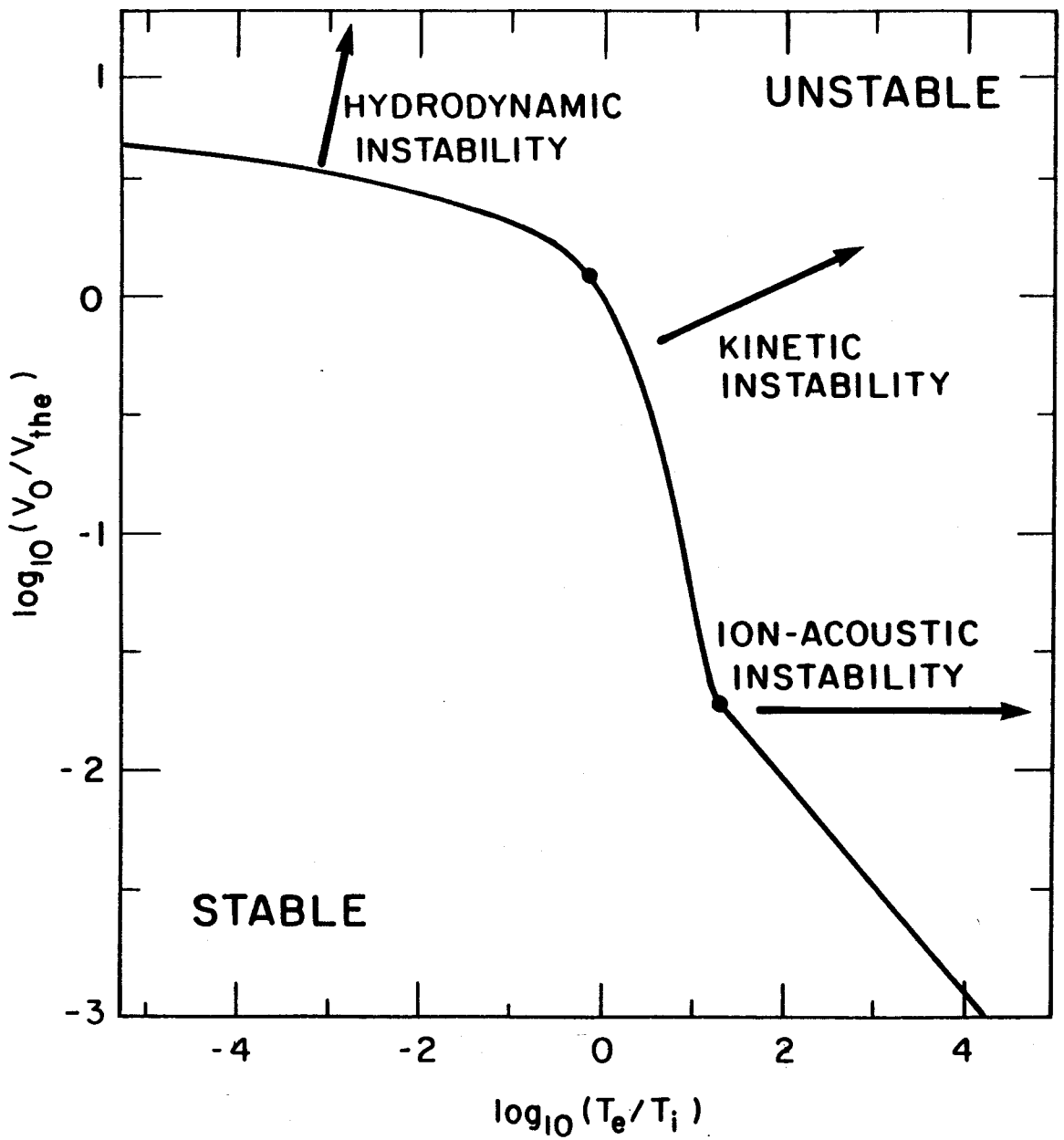
HYDRODYNAMIC
INSTABILITY
UNSTABLE
KINETIC
INSTABILITY
ION-ACOUSTIC
INSTABILITY
STABLE
1
0
-1
-2
-3
-4
-2
0
2
4
log10 (V0/Vthe)
log10 (Te/Ti)

FIGURE 5a

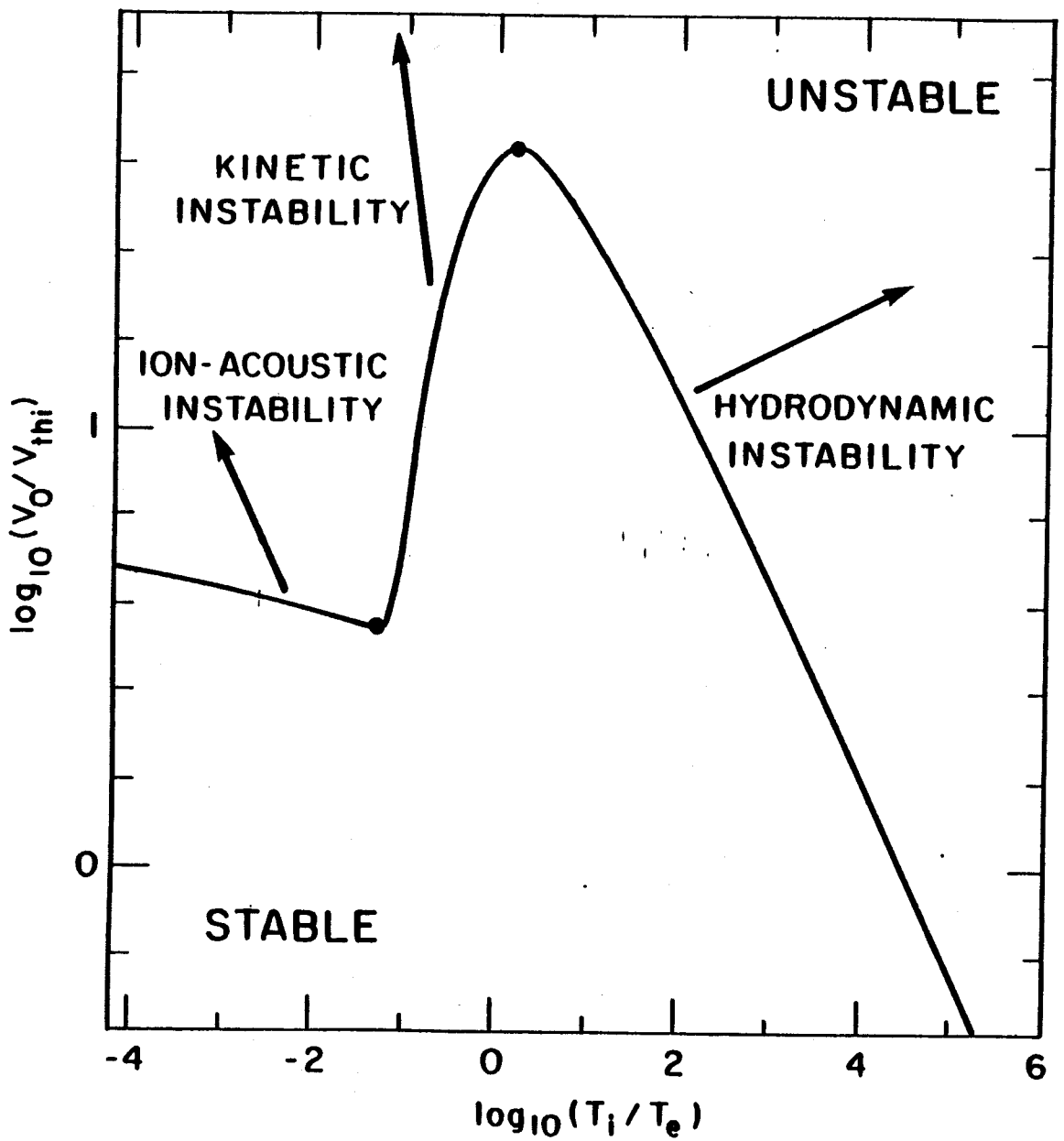
UNSTABLE
KINETIC
INSTABILITY
ION-ACOUSTIC
INSTABILITY
HYDRODYNAMIC
INSTABILITY
STABLE
1
0
-4
-2
0
2
4
6
log10(V0/Vthi)
log10(Ti/Te)

FIGURE 5b

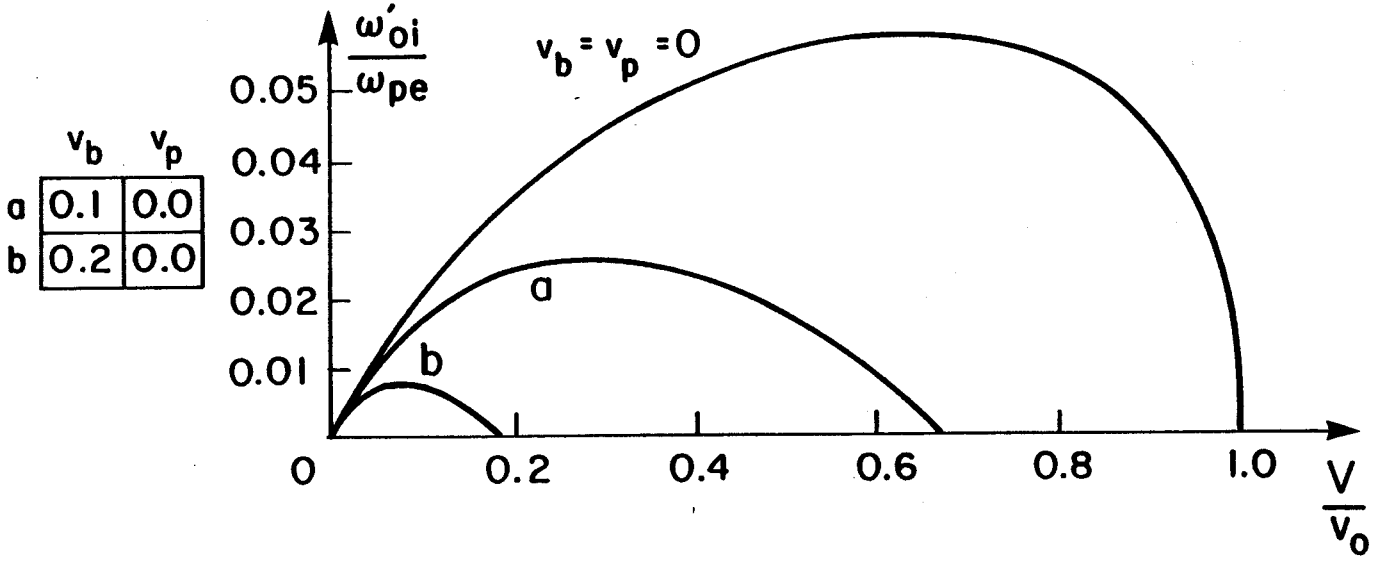
$\frac{\omega'_{oi}}{\omega_{pe}}$
$v_b = v_p = 0$
0.05
0.04
0.03
0.02
0.01
0
0.2
0.4
0.6
0.8
1.0
$\frac{V}{V_0}$
a
b
v_b v_p
a 0.1 0.0
b 0.2 0.0

FIGURE 6

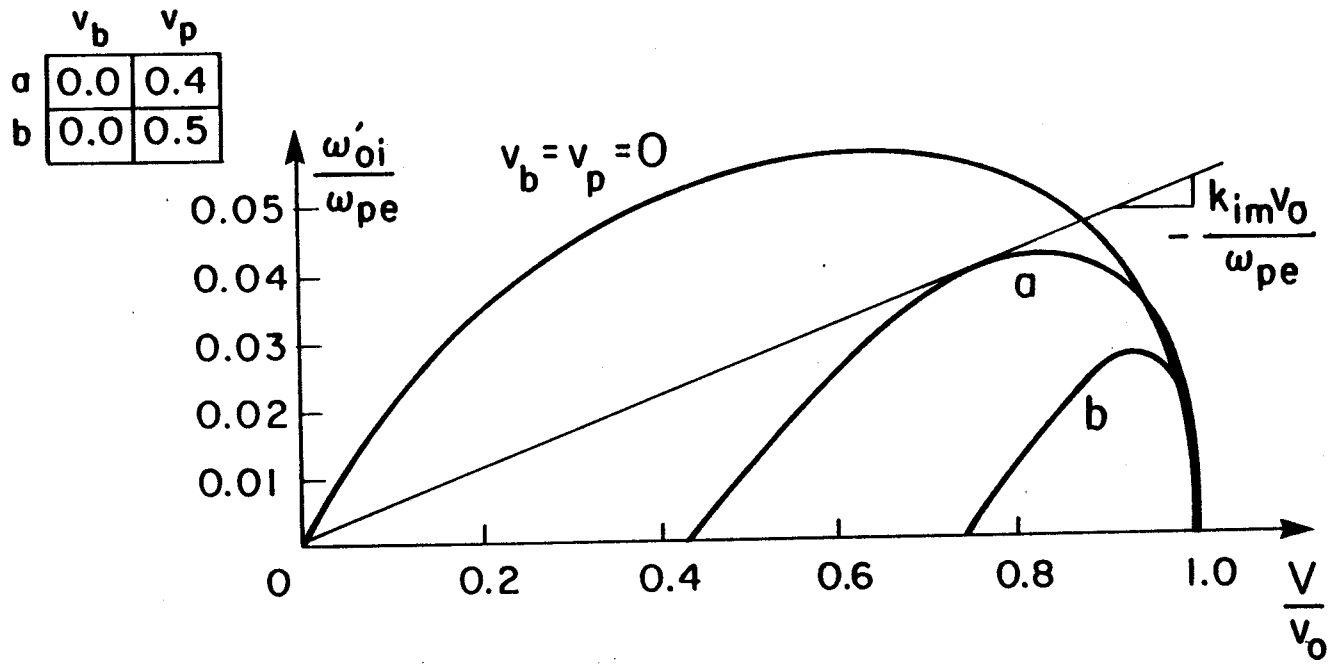
v_b v_p
a 0.0 0.4
b 0.0 0.5
$\frac{\omega'_{oi}}{\omega_{pe}}$
$v_b = v_p = 0$
$-\frac{k_{im}v_o}{\omega_{pe}}$
0.05
0.04
0.03
0.02
0.01
a
b
0
0.2
0.4
0.6
0.8
1.0
$\frac{V}{v_o}$

FIGURE 7

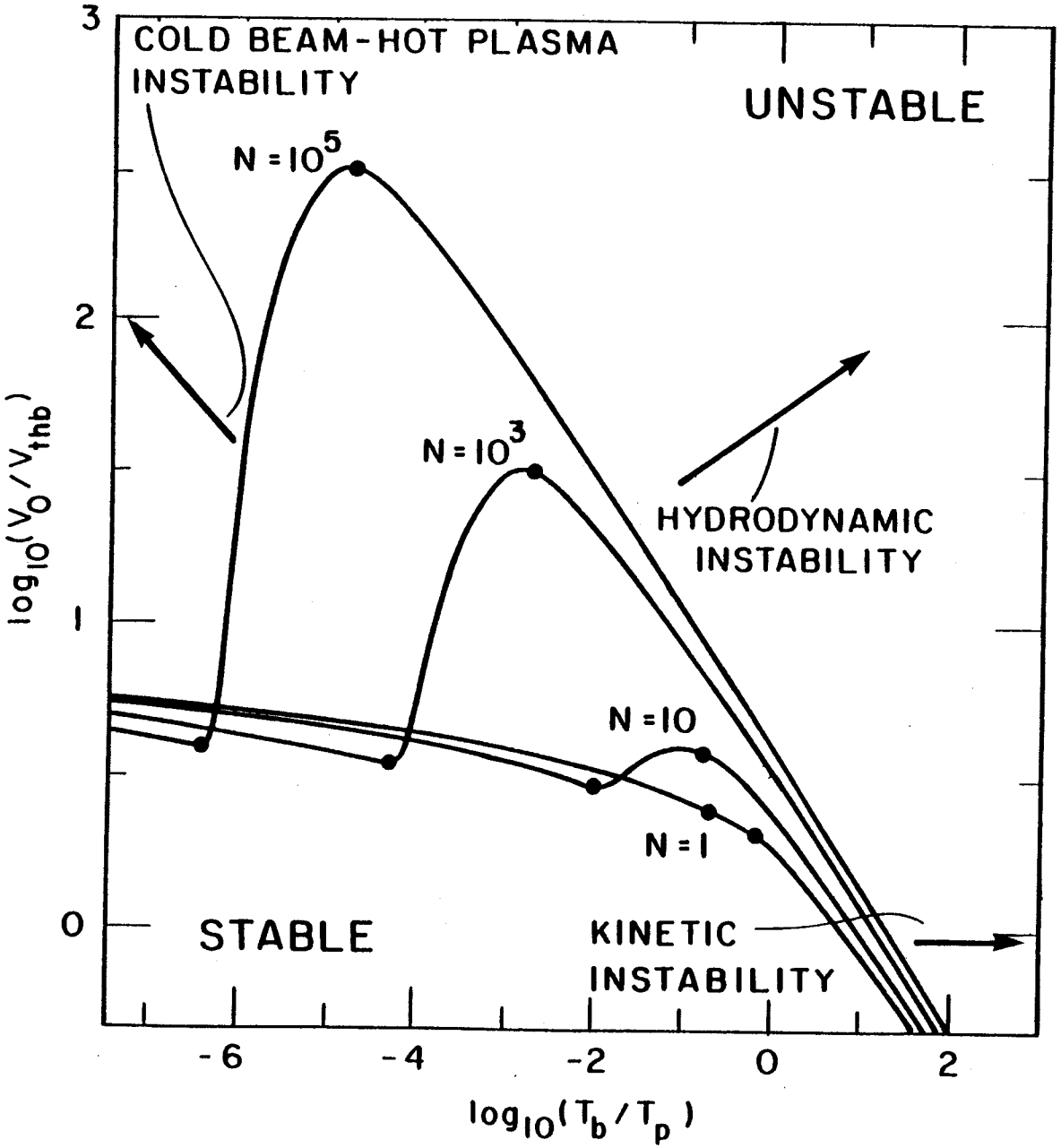
COLD BEAM-HOT PLASMA
INSTABILITY
UNSTABLE
N = 10^5
N = 10^3
HYDRODYNAMIC
INSTABILITY
N = 10
N = 1
STABLE
KINETIC
INSTABILITY
3
2
1
0
-6
-4
-2
0
2
log10(V0 / Vthb)
log10(Tb / Tp)

FIGURE 8a

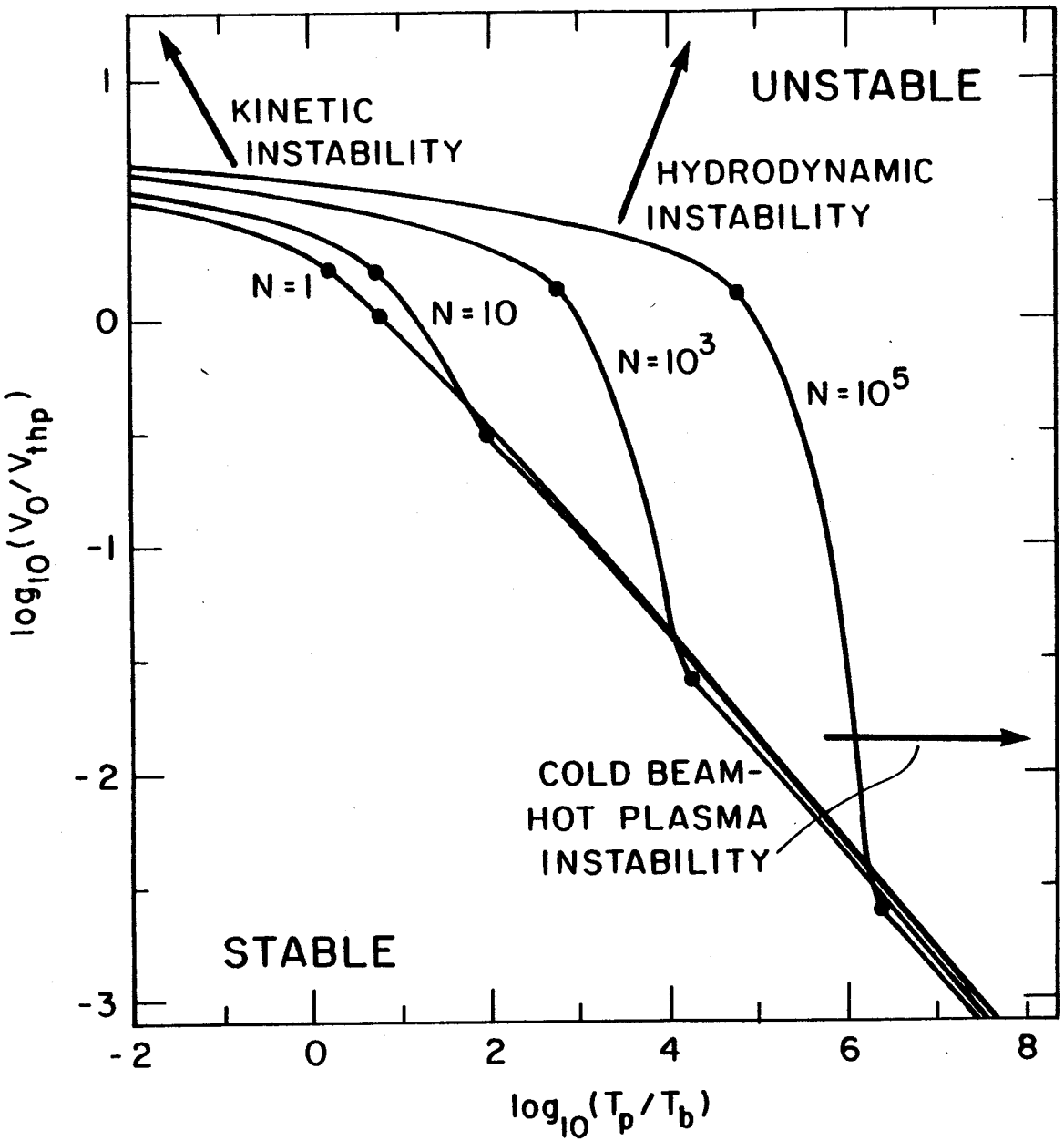
UNSTABLE
KINETIC
INSTABILITY
HYDRODYNAMIC
INSTABILITY
N = 1
N = 10
N = 10^3
N = 10^5
COLD BEAM-
HOT PLASMA
INSTABILITY
STABLE
log10(V0/Vthp)
log10(Tp/Tb)
1
0
-1
-2
-3
-2
0
2
4
6
8

FIGURE 8b

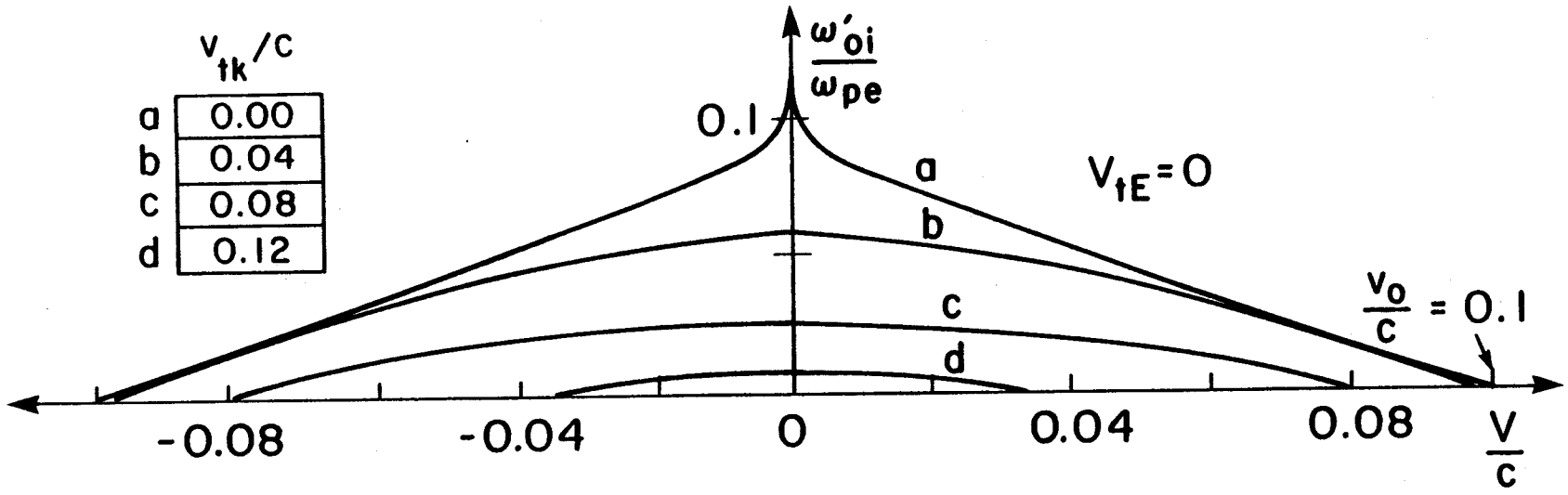
V_{tk}/c
a 0.00
b 0.04
c 0.08
d 0.12
$\frac{\omega'_{oi}}{\omega_{pe}}$
0.1
a
b
c
d
$V_{tE}=0$
$\frac{v_o}{c} = 0.1$
-0.08
-0.04
0
0.04
0.08
$\frac{V}{c}$

FIGURE 9